The permeation mechanism of potassium ions through the large conductance Ca^{2+}-activated potassium channel

Jingkang GUO[1*], Zhiyong TAN[2] Yonghua JI[1,3*,]

1: Laboratory of Neuropharmacology and Neurotoxicology, Shanghai University, Nanchen Road 333, Shanghai 200444, China.

2: Department of Pharmacology and Toxicology and Stark Neurosciences Research Institute, Indiana University School of Medicine, Indianapolis, IN, 46202, USA.

3: Xinhua Translational Institute for Cancer Pain, Chongming, Shanghai 202151, China.

Abstract

The permeation of the potassium ion (K^+) through the selectivity filter (*SF*) of the large conductance Ca^{2+}-activated potassium (*Slo1*) channel remains an interesting question to study. Although the mode of the K^+ entering and leaving *SF* has been revealed, the mechanism of the K^+ passing through the *SF* is still not clear. In the present study, the pattern of K^+ permeation through the *SF* is investigated by chemical computation and data mining based on the molecular structure of *Slo1* from *Aplysia californica.* Both bond configurations and the free energy of K^+*s* inside *SF* was studied using *Discovery Studio Software*. The results suggested that, to accommodate increasing energy levels and to tolerate more K^+s, 4-fold symmetric subunits of *SF* can only move at one direction that is perpendicular to the centre axis. In addition, two configurations of chemical bonds between K^+*s* and the *SF* are usually employed including the chelate configuration under low free energy and the complexe configuration under high free energy conditions. Moreover, three patterns of bond configurations for multiple K^+s within the SF are used to accommodate the energetic changes of

This is the author's manuscript of the article published in final edited form as:

Guo, J., Tan, Z., & Ji, Y. (2019). Permeation Mechanism of Potassium Ions through the Large Conductance Ca2+-Activated Potassium Channel. ACS Chemical Neuroscience, 10(8), 3601–3610. https://doi.org/10.1021/acschemneuro.9b00215

the *SF*, and each pattern is comprised of one or two sub-conformations. These findings are likely resulted from the evolutionary optimization of protein function of *Slo1*. The specific conductance and the voltage-gating of the *Slo1* channel can be reinterpreted with the permeation mechanism of K^+s found in the current study. The permeation mechanism of K^+s through *SF* can be used to understand the interaction between various toxins and the *Slo1* channel, and can be employed to develop new drugs targeting relevant ion channels.

Key words: molecular structure computation, ion channel, potassium ion transportation, coordination polymer, chemical kinetics, membrane potential,

Introduction

Potassium ions (K^+s) but not sodium ions are permitted to pass through *Slo1* channels selectively [1,2]. The permeation rate is close to the diffusion limit rates (10^8 ions s^{-1}) for K^+s to pass the channel pore that includes a SF of maximum diameter of 10*Å* and a 12*Å*-long, spanned by 4-fold symmetric amino-acid sequences, namely signature sequence [3-5]. The *SF* contains five layers of four in-plane oxygen atoms that point towards the ion conduction pathway under physiological conditions [6,7]. This arrangement creates a narrow tube consisting of four equally spaced ion-binding sites (labeled 1 to 4 from extracellular to intracellular side) [8]. In each binding site, a dehydrated K^+ is cross-linked to eight oxygen atoms on the vertices of the twisted cube (named a square anti-prism) [9]. The three outmost binding sites are surrounded exclusively by eight carbonyl oxygen atoms from the amino acid residuals of the signature sequence. The forth binding site, adjacent to the central pore cavity, is formed by four carbonyl oxygen atoms and four oxygen atoms of the side chain of *Thr*. In each of the binding sites, a K^+ is potentially held at the body center of the square anti-prism with one plane of four oxygen atoms above and one plane of four oxygen atoms below [10]. *SF* catalyzes the dehydration, transfer and rehydration of a K^+ in about 10 nanoseconds. The energetic balance of equivalent configuration is crucial for K^+ transportation with the near diffusion-limit rate. The central cavity holds a K^+ surrounded by eight water molecules. The cavity achieves a very high effective K^+ concentration (2*M*) at the membrane center, with a K^+ positioned on the pore axis, ready to enter *SF*. The transfer of a K^+ between the inter/extracellular solution (where a K^+ is hydrated) and *SF* (where the K^+ is

dehydrated) is mediated by a specific arrangement of carbonyl oxygen atoms that protrude into solution. The K^+ ready to enter *SF* is drawn from a fully hydrated position to a position where it is half hydrated by the electrostatic field within the filter [7].

However, an interesting problem, how K^+s are transmitted through *SF,* remains unclear. In this work, the intrinsic atom structure of a full-length*Slo1* channel from *Aplysia californica* (*acSlo1*) channel was analyzed and the free energy of K^+*s* moving through *SF* was counted with *Discovery Studio Software* [11]. The results revealed that the 4-fold symmetric signature sequences, named potassium transportation track (*PTT*), moved only in the direction perpendicular to the central axis of *SF*. In addition, it was also found that two configurations of chemical bonds between K^+*s and SF* were usually employed including chelate for low free energy and complexe for high free energy. Furthermore, three allosteric patterns of sub-conformations were found to fit the energetic changes of *SF*.

Results and Discussion

Intrinsic structure of *PTT*

The structure of *acSlo1* at 3.5*Å* has been resolved recently [12]. In this work, the intrinsic structure of ac*Slo1* was studied with *Discovery Studio Software.* The result found that each *PTT* was comprised of five residuals and contained five backbone carbonyls (*PTTBCs,* BC_{Thr}-BC_{Val}-BC_{Gly_1}- BC_{Phe}-BC_{Gly_2}) from intracellular to extracellular. Oxygen atoms of *PTTBC* (*PTTBCOs,* BCO_{Thr}-BCO_{Val}-BCO_{Gly_1}-BCO_{Phe}-BCO_{Gly_2}) toward the central axis were found to be the kernel elements for K^+ transformation.

Homologous similarity alignment found that a conserve motif of

PTT (*Thr-(Val,Ile,Leu)-Gly$_1$-(Tyr,Phe)-Gly$_2$,TXGXG)* universally occurred in various *KC-Pore*【Table 1】【**Supplement1**】. In a *PTT*, a polarity residual (*PR*) of *Thr* with a hydroxyl group was located at the first site. *Gly* at the third and fifth sites were *PR* without *R* group. These *PRs* were connected with non-polarity residuals (*nPRs*) to avoid mutual exclusion of charge. The second site was usually filled with *nPRs*, such as *Val*, *Leu* and *Ile*. These *nPRs* always contained simplistic steady-neutral group. The forth site was packed of aromatic residuals, *Phe* or *Tyr*, both of which have a big *R* group. Enough capacity for the aromatic residual was supplied by two neighbors of *Gly* to accommodate large volume of benzene ring 【Fig.1 a】. Angulations of the sequence were avoided by utilizing characterization arrangement of residuals in a *PTT*.

Table1 sequence alignment of *PTT* for various potassium channel

PDB	TYPE	SEQUENCEALIGNMENT
hSlo1A	Slo1	**V T M S T V G Y G D I F A**
acSlo1	Slo1	**V T M S T V G F G D I F A**
5A5G	Slo2.2	**V T F S T V G Y G D V T P**
1ORQ	KvAP	**V T A T T V G Y G D V V P**
3T1C	NaK	**V T L T T V G Y G N F S P**
3T4D	NAK2K	**V T L T T V G Y G D F S P**
3LUT	Kv1.2	**V S M T T V G Y G D M V P**
3LDC	MthK	**V T I A T V G Y G D Y S P**
1P7B	KirBac1.1	**E T L A T V G Y G D M H P**
3SPI	Kir2.2	**E T Q T T I G Y G F R C V**
3ZRS	KirBac3.1	**Q T M A T I G Y G K L I P**
3SYO	Kir3.2	**E T E T T I G Y G Y R V I**
5WUA	Kcnj11	**E V Q V T I G F G G R M V**
1K4C	Kcsa_fab	**E T A T T V G Y G D L Y P**
4GX2	GsuK	**T V M T T L G F G D I T F**

In the *SF* of *acSlo1,* four W-like *PTTs* were found to stand up anticlockwise around the central axis and to form a tetrahedron 【Fig.1 b】. The orientation of *PTTBCs* was counterclockwise and almost perpendicular to the plane of *PTT* 【Fig.1 c】. Absolute

values of dihedral angle ($|\lambda|$) between each pair of *PTTBCs* in a *PTT* were distributed from 164.73° to 179.05° and close to 180° 【Table 2】. It revealed that five *PTTBCs* of a *PTT* were in parallel 【Fig.1 d】. Actually, BCO_{Thr} and BCO_{Val} and BCO_{Gly_1} were positioned in a zigzag line ($ZL_{BCO_{Val}-BCO_{Gly_1}}$). BCO_{Gly_1} and BCO_{Phe} and BCO_{Gly_2} were located in another zigzag line ($ZL_{BCO_{Phe}-BCO_{Gly1}}$). Two *PTT* lines intersected at BCO_{Gly_1} with an angle of 165^0.

Table 2 dihedral angle between each *PTTBC* in a *PTT* of *acSlo1*

	BC_{Thr}	BC_{Val}	BC_{Gly1}	BC_{Phe}	BC_{Gly2}
BC_{Thr}		169.15	−178.12	179.05	164.37
BC_{Val}	169.15		−172.23	−172.77	177.11
BC_{Gly1}	−178.12	−172.23		176.88	169.42
BC_{Phe}	179.05	−172.77	176.88		178.18
BC_{Gly2}	164.37	177.11	169.42	178.18	

Six planar layers of oxygen atoms ($L_{Thr.OH}$, L_{Thr}, L_{Val}, L_{Gly_1}, L_{Phe}, L_{Gly_2}) were perpendicular to the central axis and were displayed along *SF in parallel*. Each layer contained four *PTTBCOs* at congener residuals, except the interior layer which was consisted of four hydroxyls of *Thr*【Fig.1 e1】. The configuration of planar layer was consistent with both electrophysiological records and results of electron density [7-9].

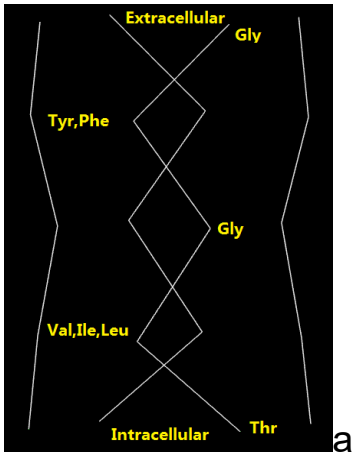

a

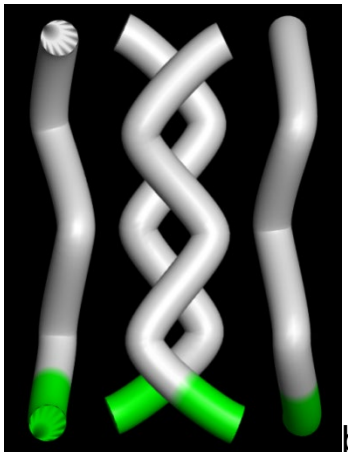
b

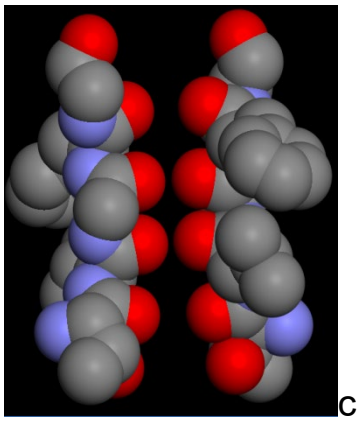
c

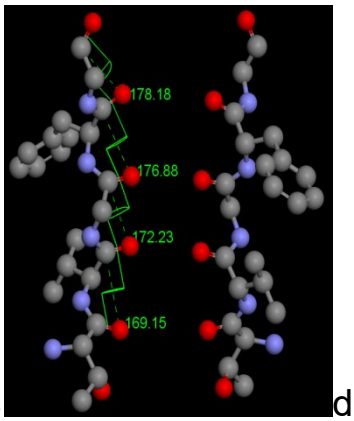

d

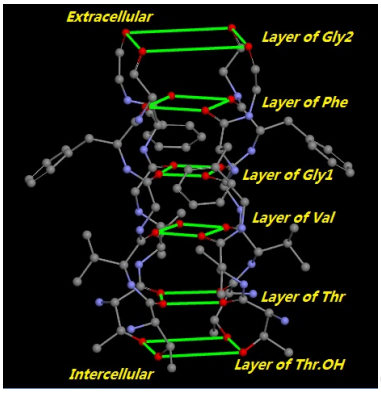

e1

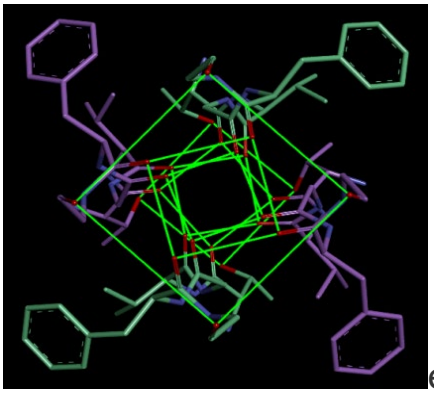
e2

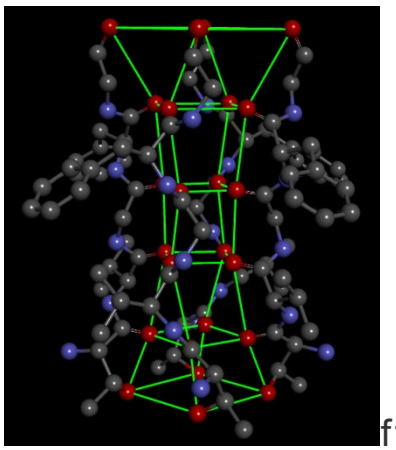
f1

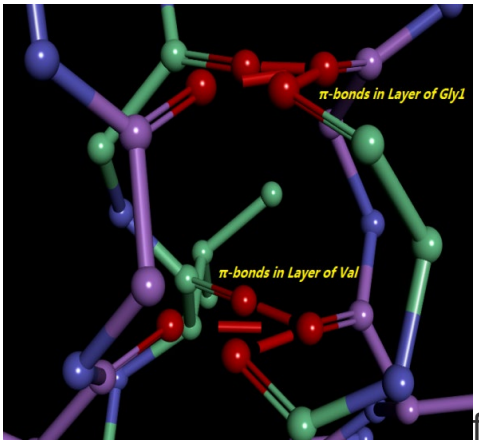

f2

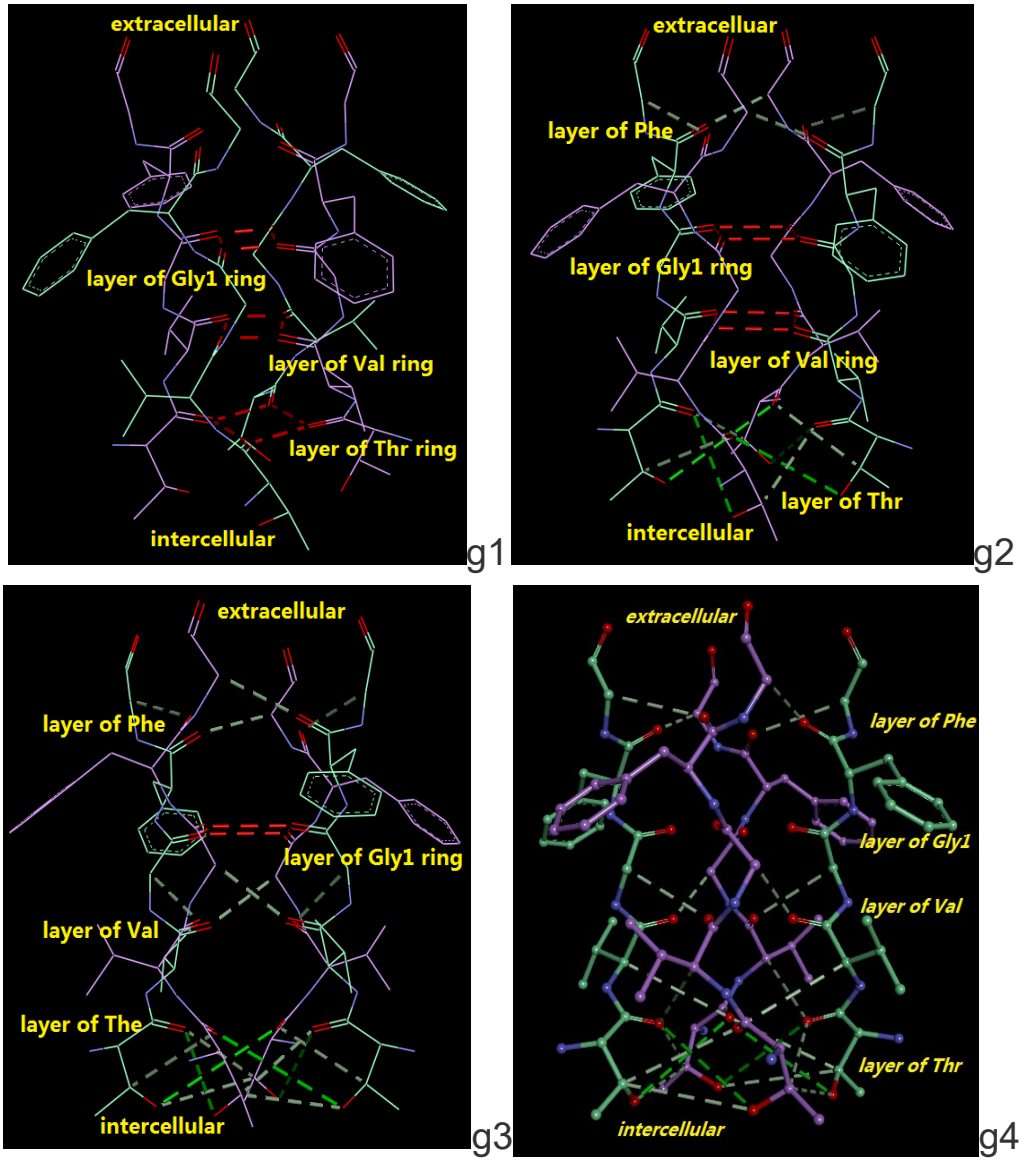

Fig.1 intrinsic structure of *PTT*:

a: A shape of stand-up anticlockwise *W* is displayed in line model of *PTT*.

b: A tetrahedron-like *PTT* is shown in tube model.

c: Two diagonal *PTTs* are shown in *CPK* model. The orientation of *PTTBCs* is at counterclockwise side and almost perpendicular to the plane of *PTT.* Red balls represent the *PTTBCOs*. Blue balls represent nitrogen atoms. Gray balls represent carbon atoms.

d: Two diagonal *PTTs* are shown in ball and stick model, of which dihedral angles between each *PTTBC* in a *PTT* are labeled. Red balls represent the *PTTBCOs.* Blue balls represent nitrogen atoms. Gray balls represent carbon atoms.

e1: Five planar layers of *PTTBCOs* and interior layer of hydroxyl of *Thr* are shown with quadrangles of light green line in stick model of tetramer *PTTs*.**e2**: The stick model of tetramer *PTTs* is viewed from external to internal.
f1:Six continual tortile-cuboids from intercellular to extracellular are surrounded and displayed with light green lines.
f2:While$dD_{Val} < 2.1285$Å, three *π* bonds are formed among one of $BCO_{Val}$and other threeBCO_{Val} at same layer.
g:Bond-links inside *SF* of *acSlo1* are displayed with various nD_{PTTBCO}. Red dashed represent ring-*π*-bond, other color dashed represent *σ* bond. **g1**: $nD_{Thr} < 2.9995$ *Å*; **g2**:$nD_{Val} < 2.9995$ *Å*;**g3**:$nD_{Gly1} < 2.9995$ *Å*;**g4**:$nD_{Gly1} > 2.9995$ *Å*.

The distance of each pair of layers (D_{layer}) for *acSlo1* was shown below:

$$(D_{Thr.OH-Thr}\ , D_{Thr-Val}\ , D_{Val-Gly1}\ , D_{Gly1-Phe}\ , D_{Tyr-Gly2}) =$$

(2.536 *Å*, 3.495 *Å*, 3.069 *Å*, 3.499 *Å*, 3.265 *Å*)

PTTBCs in a *PTT* were fixed at the linear configuration without angulations. To preserve the feature of 4-fold axial symmetry, the locations of *PTTBCs* along the central axis were fixed also. Each D_{layer} was set in steady state and the length of *SF* was about 15.864*Å*. The value was consistent with streaming potential records and X-ray crystallographic measurements, which indicated the distance between $L_{Thr.OH}$ and L_{Phe} is about a length of 12*Å* [7,13]. Otherwise, the distance of neighbor *PTTBCOs* in a *PTT* (D_{PTTBCO}) was slightly different from D_{layer} as shown below:

$$(D_{Thr.OH-BCO_{Thr}}, D_{BCO_{Thr}-BCO_{Val}}, D_{BCO_{Val}-BCO_{Gly1}}, D_{BCO_{Gly1}-BCO_{Phe}}, D_{BCO_{Phe}-BCO_{Gly2}}) =$$

(2.740 *Å*, 3.665 *Å*, 3.083 *Å*, 3.545 *Å*, 3.979 *Å*)

According to $|\lambda|$ in Table 2 and Figure 1a, the slope PTT lines were coupled with few angulations. The difference between D_{layer}

and D_{PTTBCO} was root of both inclination and angulations of two *PTT* lines to the central axis.

In each layer, a quadrangle was comprised of cross-links of neighbor *PTTBCOs*. Border length of the quadrangle (nD_{PTTBCO}) was changeable and could respond to distance of two *PTTBCOs* located at diagonal *PTTs* (dD_{PTTBCO})【Fig.1 e2】. dD_{PTTBCO} was transformable in response to the opening and closing of *SF*. The closed *SF* was intrinsically more stable. To open the *SF*, the voltage sensors must exert positive work by applying an outward lateral force near the inner helix bundle [14]. Electrophysiology records of current-voltage behavior for K^+ and its analogues had revealed that dD_{PTTBCO} was increased to accommodate ions with lager diameter, such as from value of diameter of K^+ and Tl^+ to that of NH_4^+ and Rb^+[15]. It suggested that the movement of *PTTBCO* only happened at one direction which is perpendicular to central axis of *SF*.

To keep 4-fold axial symmetry of *SF*, the ratio of nD_{PTTBCO} was fixed. The smallest nD_{PTTBCO} always occurred at the layer of BCO_{Gly_1}. Normalization of nD_{PTTBCO} was calculated with nD_{Gly1} as the unit for *acSlo1*:

$$(nD_{Thr.OH}{:}nD_{Thr}{:}\ nD_{Val}{:}nD_{Gly1}{:}\ nD_{Phe}{:}nD_{Gly2})$$

$$=(1.76,\ 1.23,\ 1.06,\ 1.00,\ 1.33,\ 2.19)$$

As a summary, the movement of *PTT* was limited by both D_{layer} and the ratio of nD_{PTTBCO}.

A cuboid was constructed with two neighboring quadrangles. The cuboid was a little tortile because of the inclination and angulations of *PTT* lines. The tortile-cuboid was similar to the square anti-prism in *Mackinnon's model* [7]. A cuboid pipeline was constituted along

the six continual tortile-cuboids arranged from intercellular to extracellular sides【Fig.1 f1】. All cross-links among *PTTBCOs* inside the cuboid-pipeline were resolved【Fig.1 g1-g4】.

A *PTTBCO* contained both two lone-pair-electrons and two unpaired-electrons meanwhile accepting *DIEPs* from peptide. The value of *DIEPs* from a *PTTBCO* to a K^+ was between 1 and 2 electrons【**Supplement 2**】. At the same time, empty orbits were remained in *PTTBCOs*, so that both covalent and coordination bonds were possible to be formed among *PTTBCOs*. According to theory of *Pauling chemical bond,* the property of the cross-links depended on both types of bonding atoms and the distance between two bonding atoms. Cross-links among *PTTBCOs* responded to changes of either dD_{PTTBCO} or nD_{PTTBCO}.

While $dD_{PTTBCO} < 2.1285\text{Å}$, cross-link appeared among every pair of *PTTBCOs* in a layer 【Fig. 1 f2】. In the case of $dD_{PTTBCO} > 2.1285\text{Å}$ and $nD_{PTTBCO} < 2.9995\,\text{Å}$, cross-link occurred between each pair of neighbor *PTTBCOs* and a circle-cross-link happened in the layer. After $nD_{PTTBCO} > 2.9995\,\text{Å}$, there was no cross-link among *PTTBCOs* in a layer, and *PTTBCOs* trended to link with carbon atoms in nearby *PTT*.

Inside *SF* of *acSlo1*, the ratio of dD_{PTTBCO} was fixed, cross-links among *PTTBCOs* were correlated with location and orientation of the *PTT* lines. While $nD_{Gly_2} < 2.9995\,\text{Å}$, five circle-cross-links, named $C_{Thr}, C_{Val}, C_{Gly_1}, C_{Phe}$ and C_{Gly_2}, exhibited from internal to external sides. The circle-cross-links gradually disappeared with the increase of nD_{PTTBCO}. When $nD_{Gly_2} > 2.9995\,\text{Å}$ and $nD_{Phe} < 2.9995\,\text{Å}$,$C_{Gly_2}$disappeared. While $nD_{Phe} > 2.9995\,\text{Å}$ and $nD_{Thr} <$

$2.9995\,Å$, C_{Phe} was absent, BCO_{Phe} linked to *β*-carbon atom of *Phe* located at clockwise *PTT*【Fig.1 g1】. As $nD_{Thr} > 2.9995\,Å$ and $nD_{Val} < 2.9995\,Å$, C_{Thr} was disappeared, BCO_{Thr} was cross-linked to both *β*-carbon atom of *Thr* at clockwise *PTT* and hydroxyl oxygen atom at anticlockwise *PTT*【Fig.1 g2】. While $nD_{Val} > 2.9995\,Å$ and $nD_{Gly1} < 2.9995\,Å$, C_{Val} was absent, BCO_{Val} linked to *β*-carbon atoms at clockwise *PTT*【Fig.1 g3】. Once $nD_{Gly1} > 2.9995Å$, no cross-link occurred among BCO_{Gly_1} 【Fig.1 g4】.

Coordination bond from *PTTBCO* to K^+ in *SF*

To understand configuration features of chemical bonds between K^+s and *SF*, K^+s were docked to *SF* of *acSlo1* with *Discovery Studio Software*. The results revealed that the K^+ was surrounded by cross-links from *PTTBCOs*. According to theory of coordination bond, a K^+ with hybridization-orbit of *d-s-p* could accept electron of ligands. Delocalized electrons were supplied by polarized *PTTBCOs*. As a result, the coordination bond was formed between *PTTBCOs* and the K^+, in which the K^+ function was an acceptor and *PTTBCOs* were regarded as ligands. In the interactions of acceptor-ligand, the *PTTBCOs* were fixed on the stationary *PTTs*. The alteration conformation of the interactions was found to depend on motion of the K^+. Different configurations of coordination polymer were employed by the K^+s positioned at various sites of the *cuboid-pipeline*.

Stabilization of the configurations was studied by comparing both symmetry and number of coordination bonds around K^+s. More symmetrical coordination bonds formed, more stable the K^+ was.

The results showed that series *stable-state-sites* arranged along the central axis of *SF*【Fig.2 a1】.

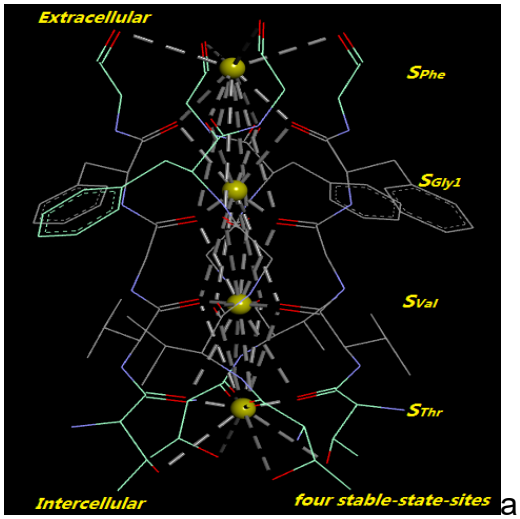

a1

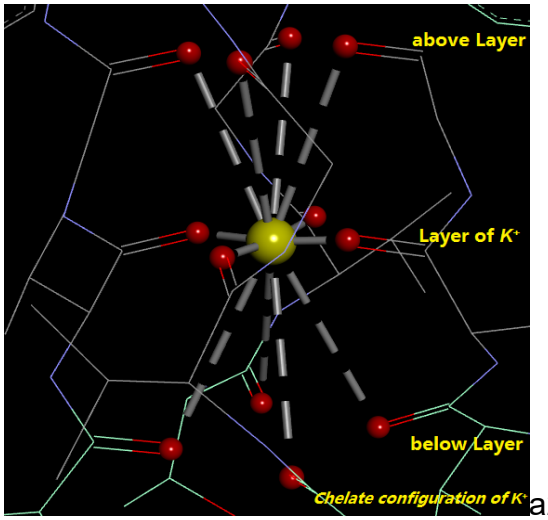

a2

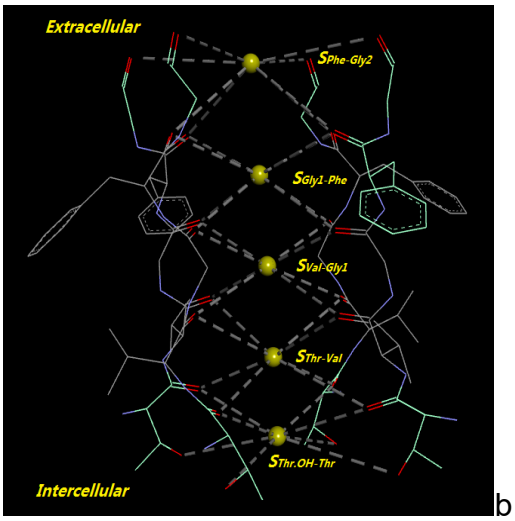

b1

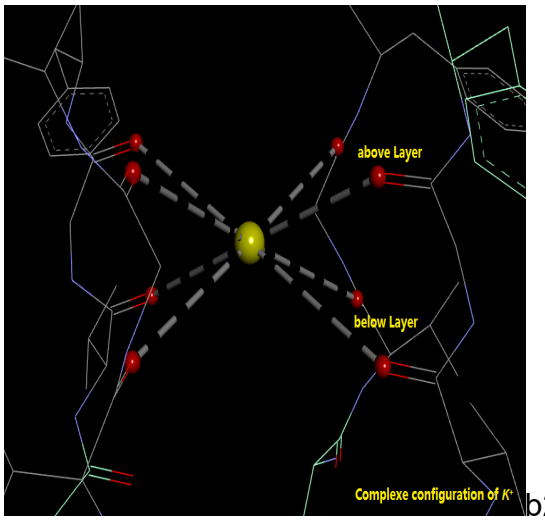

b2

Fig.2two kinds of *stable-sites* of K^+ arraying in centre axis of *SF*, yellow ball represent K^+, red ball represent oxygen atom, gray dashed represent bond between K^+ and oxygen atom.

a1: four *stable-state-sites* position along centre axis of *SF.*

a2: chelate configuration is constructed with a K^+ at the body-centered point of a dodecahedron and 12-coordination bonds: 4π-bonds to *PTTBCOs* in same layer of K^+ and 8 σ-bonds to *PTTBCOs* in above and below layers.

b1: five *meta-stable-state-sites* position along centre axis of *SF.*

b2:complexe configuration is constructed with a K^+ at body-centered point of a hexahedron and 8-coordination bonds: 4 *σ*-bonds to *PTTBCOs* in above layer and 4*σ*-bonds to *PTTBCOs* in below layer.

While nD_{PTTBCO} of a layer was smaller than $2.9995\,\text{Å}$, a *stable-state-site* occurred at the central point of the layer. The K^+ located at the *stable-state-site* was coordinated by 12 *PTTBCOs*. In the layer of K^+, *π-bonds* were formed among each pair of neighboring *PTTBCOs* so that a *ring-π-bond* with quadrilateral ligands occurred around the K^+. Delocalized electrons were supplied from the *ring-π-bond* to K^+, meanwhile were reversed from K^+ to *ring-π-bond* because of the symmetry of *SF*. It suggested that chelate bonds were formed between the *PTTBCOs* and the K^+. Furthermore, hybridization orbits of the K^+ accepted *DIEPs* from both 4 *PTTBCOs* of the above layer and 4 *PTTBCOs* of the below layer simultaneously. 8 *σ-bonds* from either the above layer or the below layer were in rotational and mirror symmetry. In the *tortile-cuboid*, the *stable-state-site* was always out of central point of the layer when nD_{Layer} was changed.

The chelate of the K^+ with maximum symmetrical coordination bonds was the steadiest state inside *SF*【Fig.2 a2】. The chelate occupying two continual *tortile-cuboids* looked like a square antiprism surrounding the K^+. A *body-centered-cube* of monoclinic system was constituted by two continual *tortile-cuboids*, which contained 8 *PTTBCOs* from both the above and the below layers. The K^+ locating at any site of the *body-centered-cube* trended to come back to the *stable-state-site*. On the other hand, three layers of *PTTBCOs* were employed by the chelate of the K^+. Two continual chelates were impossible to overlap because bonding electrons were mutually exclusive. To prevent overlapping of two continual chelates, two layers with *ring-π-bond* were separated by a layer without *ring-π-bond.* It suggested that two neighboring K^+*s*

at the *stable-state-site* were necessary to be separated by a *tortile-cuboid*.

4 *stable-state-sites* were linearly displayed along center axis of *SF*, labeled as $(S_{Thr}, S_{Val}, S_{\mathrm{Gly}_1}, S_{Phe})$, corresponding to L_{Thr}, L_{Val}, L_{Gly_1} and L_{Phe}, 【Fig.2 a1】. The result was consistent with the one-dimensional electron density obtained by sampling the difference in Fourier omit map [8]. The outmost BCO_{Gly_2} were infiltrated in external solution and dD_{Gly_2} was larger than other dD_{PTTBCO}. It looked like an opening mouth of *SF*. While $nD_{Gly_2} \cong 2.9995$ *Å*, $nD_{Gly1} \cong 1.369$ *Å*, the K^+ was forbidden by four BCO_{Gly_1} to pass through *SF*. In open state of *SF*, dD_{Gly_2} was too large for K^+ to form *ring-π-bond*. The K^+ at the center point of L_{Gly_2} was half-hydrated with 4 *σ-bonds* to BCO_{Gly_2} and some other bonds to water molecules. The identical molecular structure was suitable for the K^+ to be released from *SF* to external solution. At the internal entrance, the *hydroxyl-oxygen-atoms* of *Thr* were protruded into the internal solution. The K^+ in internal solution was easy to be caught, and a half-hydration conformation of the K^+ was formed with both 4 water molecules and 4 *hydroxyl-oxygen-atoms*. The special configuration was suitable for the K^+ to be transferred from internal solution into *SF*.

While nD_{PTTBCO} of a layer is larger than 2.9995 Å, *ring-π-bonds* were impossible to be formed and a *meta-stable-state-site* occurred at the body-center of the *tortile-cuboid*. A K^+ at the *meta-stable-state-site* was coordinated with 8 symmetrical *PTTBCOs* to form complexe of K^+ including 4 *σ-bonds* from the above layer and 4 *σ-bonds* from the below layer【Fig.2 b2】. Free energy of a K^+ at the *meta-stable-state-site* was higher than that at

the *stable-state-site*. 5 *meta-stable-state-sites* were linearly arrayed along the central axis of *SF*, labeled as ($S_{Thr.OH-Thr}$,$S_{Thr-Val}$,$S_{Val-\mathrm{Gly}_1}$,S_{Gly_1-Phe},$S_{Phe-Gly_2}$) . According to the feature of the *PTTBCOs, K*$^+$s located at the *meta-stable-state-sites* were continuous inside *SF*【Fig.2 b1】.

Conformation of *K*$^+$ inside *SF*

To interpret the pattern of *K*$^+$ transformation, trajectory of *K*$^+$ passing through *SF* was simulated with *Discovery Studio Software*. Some rules were abided by in the simulation. First, *coulomb repulsion* was the main interactive force between two *K*$^+$s inside *SF*, and *K*$^+$s were pushed to move one by one without gap. The *SF* was filled with *K*$^+$*s* as many as possible. At the same time, there was no overlap among configurations of *K*$^+$s because electron clouds were mutually excluded.

Second, because asymmetric bond-links caused unbalance interaction of *K*$^+$s with SF, *K*$^+$s with asymmetric bond-links maintained higher free energy and resided in the *unstable-state-sites of SF*. Symmetry of bond-links around *K*$^+$s at *meta-stable-state-sites* was larger than that at *unstable-state-sites* but smaller than that at *stable-state-sites*, free energy of *K*$^+$s at *meta-stable-state-sites* was higher than that at *stable-state-sites* but lower than that in *unstable-state-sites*. Most sites in *SF* were unstable with higher free energy except *stable-state-sites* and *meta-stable-state-sites*. Probability of *K*$^+$s at *meta-stable-state-sites wa*s smaller than that at *stable-state-sites,* and larger than that at *unstable-state-sites*. *K*$^+$s tended to occupy *stable-state-sites* and *meta-stable-state-sites* rather than *unstable-state-sites*.

In the case of *SF* opening under normal physiological conditions, allosteric conformations of *K*$^+$s in a scene were observed according

to the rules. While $nD_{Phe} \cong 2.9995\,Å$, a combination of two chelates and one complexe of *K*$^+$s was found inside *SF*. There were two potential sub-conformations. In one sub-conformation, two *K*$^+$*s* sat at S_{Thr} and S_{Gly_1} respectively and another *K*$^+$ sat at $S_{Phe\text{-}Gly_2}$. This sub-conformation was labeled as [S_{Thr}-S_{Gly_1},$S_{Phe\text{-}Gly_2}$] 【Fig.3 a】. In the other sub-conformation, a *K*$^+$ sat at $S_{Thr.OH\text{-}Thr}$ and two other *K*$^+$*s* sat at S_{Val} and S_{Phe} respectively. This sub-conformation was labeled as [$S_{Thr.OH\text{-}Thr}$, S_{Val}-S_{Phe}] 【Fig.3 b】. The energy of these sub-conformations was equilibrium. When $nD_{Thr} \cong 2.9995\,Å$, two possible sub-conformations were mixed with chelates and complexes of *K*$^+$. One sub-conformation was [S_{Thr}-S_{Gly_1},$S_{Phe\text{-}Gly_2}$] as described above【Fig.3 a】. In the other sub-conformation, three *K*$^+$*s* sat at $S_{Thr.OH\text{-}Thr}$, $S_{Gly_1\text{-}Phe}$ and $S_{Phe\text{-}Gly_2}$ respectively and another *K*$^+$ sat at S_{Val}. This sub-conformation was labeled as [$S_{Thr.OH\text{-}Thr}$, S_{Val}, $S_{Gly_1\text{-}Phe}$- $S_{Phe\text{-}Gly_2}$]【Fig.3c】. As $nD_{Val} \cong 2.9995\,Å$, there were two sub-conformations including the [$S_{Thr.OH\text{-}Thr}$, S_{Val}, $S_{Gly_1\text{-}Phe}$- $S_{Phe\text{-}Gly_2}$]【Fig.3c】and similarly the [$S_{Thr.OH\text{-}Thr}$- $S_{Thr\text{-}Val}$, S_{Gly_1}, $S_{Phe\text{-}Gly_2}$]【Fig.3d】. These sub-conformations were coincided with the records of two-dimensional infrared (*2D IR*) spectroscopy [16]. When nD_{Val} and nD_{Gly_1} were over $2.9995\,Å$, there were five complexes of *K*$^+$ inside SF. And the sub-conformation was labeled as [$S_{Thr.OH\text{-}Thr}$- $S_{Thr\text{-}Val}$- $S_{Val\text{-}\mathrm{Gly}_1}$- $S_{Gly_1\text{-}Phe}$- $S_{Phe\text{-}Gly_2}$]【Fig.2 b1】. This sub-conformation agreed with the *2Fo - Fc* electron density map [7] and *2D IR* spectroscopy [16].

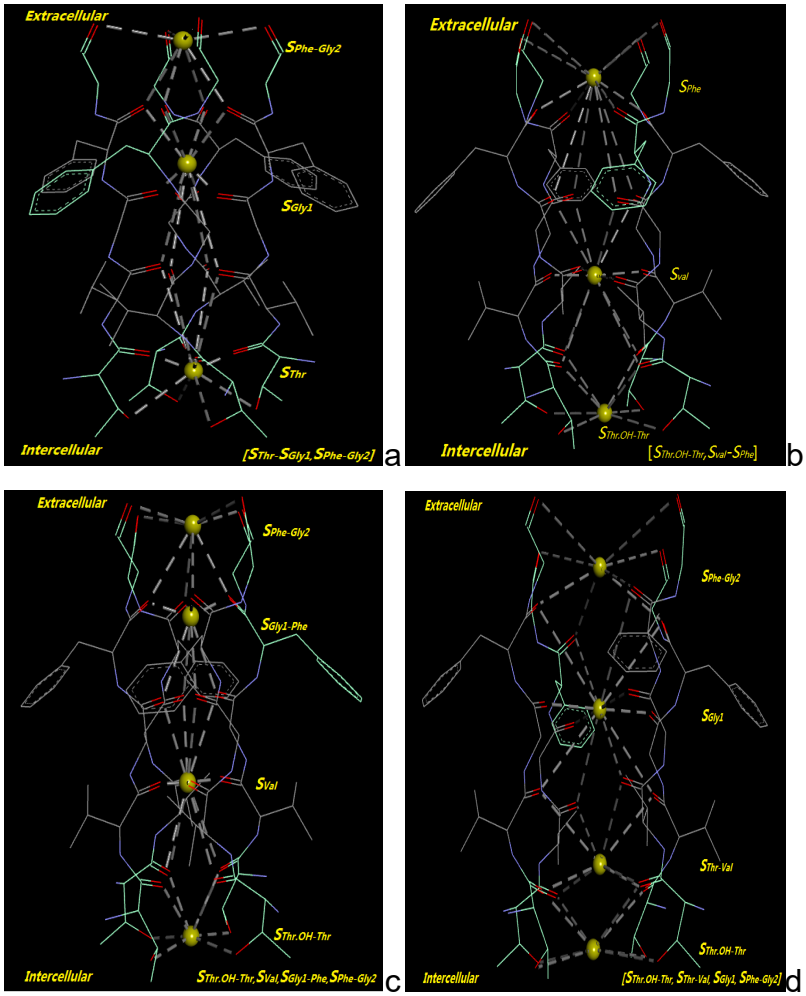

Fig.3 Pattern of K^+ transportation inside *SF*, yellow ball represent K^+, gray dashed represent bond around K^+

a,b: pattern 1, including two sub-conformations, each of which contains a chelate configuration and two complexes configurations;

c,d: pattern 2, including two sub-conformations, each of which contains a chelate configuration and three complexes configurations.

All sub-conformations of K^+ in *SF* were summarized and clustered into three patterns: 1) $[S_{Thr.OH\text{-}Thr}, S_{Val}\text{-}S_{Phe}]$ and $[S_{Thr}\text{-}S_{Gly_1}, S_{Phe\text{-}Gly_2}]$; 2) $[S_{Thr.OH\text{-}Thr}, S_{Val}, S_{Gly_1\text{-}Phe}\text{-}S_{Phe\text{-}Gly_2}]$ and $[S_{Thr.OH\text{-}Thr}\text{-}S_{Thr\text{-}Val}, S_{Gly_1}, S_{Phe\text{-}Gly_2}]$; 3) $[S_{Thr.OH\text{-}Thr}\text{-}S_{Thr\text{-}Val}\text{-}S_{Val\text{-}Gly_1}\text{-}S_{Gly_1\text{-}Phe}\text{-}S_{Phe\text{-}Gly_2}]$. The pattern of

sub-conformations changed according to the energy level of the *Slo1* channel. The sub-conformations in pattern 1 with a complexe and two chelate configurations were employed to suit the lower energy of *Slo1* channel. When the energy level of the *Slo1* channel was medium, dD_{PTTBCO} was enlarged to tolerate more K^+*s* and therefore a chelate configuration was replaced by two complexe configurations, resulting in 4 configurations in the pattern 2. When the energy level of the *Slo1* channel was high, another chelate configuration was split into two complexe configurations, resulting in five K^+*s* in *SF* with the largest dD_{PTTBCO} in pattern 3. The changes of sub-conformations were consisted with *Mackinnon's* model, and were crucial to the operation of *SF* in the cellular context [10].

Energy gradient for K^+ transporting through *SF*

The ability for K^+s to form coordination polymer is rooted in both energy levels of *d* orbit splitting and of *d-s-p* orbit hybridizing. The orbit distribution of extra-nuclear electron for a K^+ is $3d4s^14p$. Energy level of *d* orbit is split from group $K(z)$ to group $D_{4d}\left[\mathrm{e}_3\left(\mathrm{d_{xz}},\mathrm{d_{yz}}\right),\mathrm{e}_2\left(\mathrm{d_{xy}},\mathrm{d_{x^2-y^2}}\right),\mathrm{a}_2\left(\mathrm{d_{z^2}}\right)\right]$, and then to group $O\hbar$ $\left[\mathrm{t}_{2\mathrm{g}}\left(\mathrm{d_{xy}},\mathrm{d_{xz}},\mathrm{d_{yz}}\right),\mathrm{e_g}\left(\mathrm{d_{z^2}},\mathrm{d_{x^2-y^2}}\right)\right]$ corresponding to symmetry of ligand-field decreases. The energy-level-split orbit is hybridized with either *s* or *p* orbit to form hybridization-orbit, such as d^5p^3 and d^5sp^2.

According to ligand-field theory, the number of ligands responds to the free energy of the K^+. An icosahedron is suitable for group $K(z)$ of K^+ with minimum free energy. A *body-centered-cube* of monoclinic system fits group D_{4d} as the free energy of K^+ increases. And group *Oh* of K^+ with high free energy is satisfied by

a cube. For example, an icosahedron with water molecules usually occurs to suit minimum free energy of K^+ in the extracellular solution with low K^+ concentration and a cube with 8 water molecules always occur to fit high free energy of K^+ in the intercellular solution with high K^+ concentration. Within the *SF*, the K^+ with low free energy prefers a chelate configuration with 12 coordination bonds, and a complexe configuration with 8 *σ-bonds* trends to be employed by the K^+ with high free energy.

Furthermore, at the internal side of *SF*, there is a very high effective concentration of K^+ (2M). The K^+ is surrounded by 8 water molecules. The unique picture of a hydrated K^+ results from a geometric and chemical match between the cavity and the hydration complexe of the K^+. While crossing the internal threshold of *SF*, a K^+ comes through fully-hydrated, half-hydrated and dehydrated state. This process is achieved with help of four *hydroxyl-oxygen-atoms* at side-chain of *Thr*, which protrude into the internal solution [17]. The translocation of a K^+ from the internal solution into *SF* is an active process that is driven by chemical potential gradient. At external side of *SF*, an icosahedron of water molecules is rendered for K^+ with 20-coordinations in minimum concentration (3~5mM). As crossing the external threshold of *SF*, a K^+ undergoes dehydrated, half-hydrated and rehydrated states. This process is mediated by four BCO_{Gly_2} with large nD_{Gly_2}. The translocation of a K^+ from *SF* to the extracellular solution is also an active process, which is driven by the diffusion force resulted from chemical potential gradient. Inside *SF*, the entering of a K^+ entering into a *stable-state-site* is an active process, in which a variable accelerated motion of the K^+ occurs with motive power resulted from the free energy decline. On the contrary, the escape of a K^+

from a *stable-state-site* is a passive process with variable decelerated motion. A K^+ undergoes the dehydration, transportation and rehydration inside *SF*. The translocation of a K^+ from internal threshold to external threshold is driven by recombination kinetics of both chemical potential gradient and membrane voltage potential.

In either pattern 1 or pattern 2, three or four K^+*s* move in a concerted fashion between two sub-conformations until a new K^+ enters to displace a K^+ on the opposite side. The two sub-conformations are in alteration and in equilibrium of energy in the transportation of K^+. The alteration of two sub-conformations is consisted with *Mackinnon's* model [10]

Recombination kinetic for K^+ transporting

A vector function of recombination kinetics ($\overrightarrow{RK}$) for K^+ in *SF* resulted from the chemical dynamics analysis is as below:

$$\overrightarrow{RK} = \overrightarrow{CP} + \overrightarrow{EP} = \Theta\left(\overrightarrow{CP_{ion}}\right) + \left(\overrightarrow{EP_{out}} + \sum_{ion} \overrightarrow{EP_{ion}}\right) \qquad (4)$$

$\overrightarrow{CP}$: represents diffusion force of ion concentration, which interacts with congener ion-itself. The value of $\overrightarrow{CP}$ is vector function of chemical potential gradient and given by *Nernst-Frank* function as shown as following [18,19]:

$$\overrightarrow{CP} = \Theta\left(\overrightarrow{CP_{ion}}\right) = \Theta\left(\left(\frac{RT}{F} ln \frac{[Ion]_o}{[Ion]_i}\right)_{ion}\right) \qquad (5)$$

R: gas constant, 8.3143 J/(K·mol)

T: abstract temperate K

F: faraday constant, $9.6485*10^4$ C/mol

$[Ion]_o$: external ionic activity

$[Ion]_i$: internal ionic activity

$\overrightarrow{EP}$: represents electric potential force, which is a vector component value on *SF* resulting from cellular membrane voltage ($\overrightarrow{mV}$). Accumulation of inter/extracellular ions are shown as following:

$$\overrightarrow{EP} = \overrightarrow{EP_{out}} + \sum_{ion} \overrightarrow{EP_{ion}} = \overrightarrow{EP_{out}} + \frac{RT}{F} ln \frac{\sum_{ion}[Ion]_o}{\sum_{ion}[Ion]_i} \quad (6)$$

$\overrightarrow{EP_{out}}$: represents additional electric potential on cellular membrane.

In vector computation of $\overrightarrow{RK}$, positive direction is defined at extracellular. At physiology condition, $\overrightarrow{EP_{out}} = 0$, the value of $\overrightarrow{RK}$ for K^+ is shown as below:

$$\overrightarrow{RK}_{K^+} = \left|\overrightarrow{CP}_{K^+}\right| + \sum_{ion} \overrightarrow{EP_{ion}} = \left|\frac{RT}{F} ln \frac{[K^+]_i}{[K^+]_o}\right| - \frac{RT}{F} ln \frac{\sum_{ion}[Ion]_o}{\sum_{ion}[Ion]_i} \cong 0$$

According to *Hodgkin-Huxley assumption* [20,21], conductance of K^+ (g_{K^+}) is given by the following equation:

$$g_{K^+} = \overline{g_{K^+}} * \frac{d\overrightarrow{RK}_{K^+}}{dx} \quad (7)$$

$\overline{g_{K^+}}$: represents a intrinsic conductance constant, that is decided by total energy of sub-configurations in *SF*. $\overrightarrow{RK}_{K^+}$ is a function of position. Current of K^+ (I_{K^+}) is shown as below equation:

$$I_{K^+} = \overrightarrow{RK}_{K^+} * \int \overline{g_{K^+}} * \frac{d\overrightarrow{RK}_{K^+}}{dx} \quad (8)$$

Under physiological conditions, K^+*s* diffuse via *SF* at rates approaching 10^8 ions/s [10]. It means that 10 nano-seconds are consumed for a K^+ to pass through *SF*. However, according to Newtonian mechanics, theoretical time for K^+ freely flying cross *SF* with length of 15.864*Å*, is about 2.48 pico-seconds **【Supplement 3】**. Actual time for a K^+ spent in *SF* is longer than the theoretical

time. That means the K^+ is far from the state of free moving driven by the electric field between the inter/external sides of *SF*. The conductivity of *SF* is a chemical reaction limiting parameter. It is restricted by the slowest step of the K^+ escaping from the *stable-state-sites*. In theoretical statement, a K^+ is forbidden in the *stable-state-sites* when *SF* is in polarization. $\overrightarrow{RK}_{K^+}$ continually increases while *SF* begins to be depolarized. After $\overrightarrow{RK}_{K^+}$ is raised over potential barrier of the *stable-state-sites*, it is possible for K^+ to escape from the *stable-state-sites* and to be transmitted from intercellular to extracellular sides. The K^+ permeability is decided by both the configuration of the K^+ in the *stable-state-sites* and the combinational pattern of sub-conformations.

The role of waters in the moving of K^+ through the SF

The role of water molecules inside SF has been studied by the detection of streaming potential in the *Slo1* channel [13]. In this study, K^+ coupled with water molecules has been used as a prerequisite in the discussion of streaming potential records. In *Mackinnon's* model that is constructed based on synchrotron crystals and electron density, two K^+s with diameter of 2.7*Å* are assumed to be separated by an intervening water molecule to avoid an unstable binding configurations resulting from coulomb repulsion. However, it is difficult to distinguish electron density of

K^+s from that of water molecules in X-ray crystallographic. In this model, the K^+s pair moves back and forth in a concerted manner between two configurations of minimal energy difference, namely K^+-water-K^+-water(1-3 configuration) and water-K^+-water-K^+ (2-4configuration) [17]. A*2D IR* spectra are reproduced by *MD* simulations of structures with waters separating two K^+s in *SF* [16]. The results rule out the configurations with K^+ occupying adjacent sites on the one hand. On the other hand, it is still in doubt whether or not water molecules are actually inside *SF*.

Motivation is an important factor for water molecule to pass through *SF*. Water molecules are independent of K^+s inside *SF* because K^+s are dehydrated inside *SF.* Under $\overrightarrow{RK}$ of the *Slo1* channel, neutral water molecules without charges are impossible to be driven and to pass through *SF*. In water molecules, hydrogen hydrate ions are potential components that can be transmitted through the electro-negativity field of *SF.* And the hydronium (H_3O^+) seems to be the only cation with a suitable diameter for dD_{PTTBCO} according to the *Coordination bond Theory*. However, hydronium with sp^3 orbit hybridizing tends to form a tetrahedron rather than an octahedron or a dodecahedron. Therefore, hydronium is hard to be transferred along the *SF* based on their coordination with *PTTBCOs*. Indeed, it suggests that permeation capability of water

molecules is similar to that of sodium ion, and is far smaller than that of K^+ inside *SF*.

On the other hand, a comparison of atomic structure between the *Mackinnon's* model and the pattern 1 conformation of the current study reveals that the configurations of the *Mackinnon's* model seem to be part of sun-conformations of pattern 1 conformation in this study. 1-3 configuration of the *Mackinnon's* model corresponds to combine *stable-state-sites* of S_{Val}- S_{Phe} in $[\mathrm{S}_{Thr.OH\text{-}Thr}, S_{Val}\text{-}\ S_{Phe}]$ and 2-4 configuration of the *Mackinnon's* model corresponds to combine *stable-states-sites* of S_{Thr}- $\mathrm{S}_{\mathrm{Gly}_1}$ in $[\mathrm{S}_{Thr}\text{-}\ \mathrm{S}_{\mathrm{Gly}_1}, S_{Phe\text{-}Gly_2}]$. Chelate configurations are employed and it is found that two K^+s are separated by a tortile-cuboid rather than a water molecule.

Furthermore, a survey of a database of small-molecule structure (Cambridge Crystallographic Data Centre, http://www.ccdc.cam.ac.uk) shows that two K^+s rarely occur with a separation distance of less than 3.5*Å*. In sun-conformation of [$\mathrm{S}_{Thr.OH\text{-}Thr}$- $S_{Thr\text{-}Val}$- $\mathrm{S}_{Val\text{-}\mathrm{Gly}_1}$- $S_{Gly_1\text{-}Phe}$- $S_{Phe\text{-}Gly_2}$], when dD_{PTTBCO} increases, $S_{Gly_1\text{-}Phe}$ and $S_{Phe\text{-}Gly_2}$ are shifted toward extracellular, at the same time, $S_{Thr\text{-}Val}$ and $\mathrm{S}_{Thr.OH\text{-}Thr}$ are drifted toward intercellular. C*oulomb* repulsion among five continual K^+s is avoided by displacement of the *meta-stable-state-sites*. In

summary, the present study suggests that water molecules are not necessary to be transmitted with K^+s in *SF* of the *Slo1* channels.

Experiment

Calculation of intrinsic atom structure of *PTT* in *acSlo1*

Molecular structure parameters of *SF* in *acSlo1* are calculated in *Discovery Studio Software*. Computational process for dihedral angle between each pair of *PTTBCs* is as following：1）carbon atoms and oxygen atoms of two *PTTTBCs* are selected; 2）push the button of “Structure-Monitor-Torsion” in drop-down menu, and acquire the value of dihedral angle. Computational process for D_{layer} is as following: 1) link two pair of diagonal *PTTBCOs* in a layer and get the intersection; 2) link the intersections at two neighboring layers; 3) push the button of “Structure-Monitor-Distance” in drop-down menu, and acquire the value of D_{layer}. Computational process forD_{PTTBCO} is as following: 1) select two neighboring *PTTBCOs* in a *PTT*; 2) push the button of “Structure-Monitor-Distance” in drop-down menu, and acquire the distance of D_{PTTBCO}. Computational process for nD_{PTTBCO} is as following: 1) select two neighboring *PTTBCOs* in a layer; 2) push the button of “Structure-Monitor-Distance” in drop-down menu, and acquire the value of nD_{PTTBCO} ; 3) nD_{PTTBCO}/nD_{Gly1} for each layer is calculated.

Simulation and clustering of cross-links among *PTTS* of *SF*

States of cross-links among *PTTs* of *SF* are simulated in *Discovery Studio Software*. Algorithm of homology model is employed in the simulation of calculation, and the algorithm of cluster analyze is used in the classification of cross-links. Computational process is listed step by step as following: 1) 4-fold symmetrical subunits of *acSlo1* channel are moved away from the central point synchronously at the direction perpendicular to the central axis, so that dD_{PTTBCO} varies from 2*Å* to 15*Å*. Every molecular structure of *Slo1* channel with various value of dD_{PTTBCO} is employed to be template for homology models rebuilding. 2) Push the button of "macromolecules-create homology models-build homology models" and construct homological model with various value of dD_{PTTBCO}. 3) For every rebuilding homology model, push the button of "Macromolecules-Dock and analyze protein complexes-calculate ligand interface" and analyze the cross-links between each pair of *PTTs*. 4) Changes of cross-links among *PTTs* corresponding to various dD_{PTTBCO} are compared and recoded in details. 5) All statements of cross-links are clustered, and features of cross-links in each statement are classified. 6) Every kind of cross-links is identified according to its feature.

Construction of coordination conformation for the K^+ inside SF and trajectory simulation of the K^+ passing through *SF*

The configuration of a K^+ in *SF* is imitated with *Discovery Studio Software*. Algorithm of CDOCKER and feature cluster are employed and the computational process is listed step by step as following： 1) Select the window of “Receptor-ligand interactions-view interactions”, define K^+ as receptor and *PTTBCOs* as ligand. 2) Define and edit the binding site. 3) Push the button of “Receptor-Ligand interactions-dock ligand (CDOCKER)” and dock a K^+ to *SF* in each binding site. 4) Push the button of “Receptor-ligand interactions-view interactions-analyze ligand poses”, view the receptor-ligand interactions and display the surface of receptor and ligand, and free energy of K^+s is calculated and recorded. 5) Push the button of "structure-monitor", the features of cross-links, such as orientation, torsion, length and so on, are recorded in details. 6) Push the button of "simulation-electrostatics potential", forces on K^+, such as symmetry, balance and kinetics, are analyzed and recorded. 7) The kinds of bonds around the K^+ are estimated according to the feature of cross-links.8) The configuration of K^+ is constructed with all bonds around the K^+.

Furthermore, the process of simulation of K^+ passing through *SF* is listed step by step as following: 1) Push the button of "simulation-calculate interaction energy", calculate and compare free energy of every conformation of K^+, steady-states of K^+ with low free energy are labeled. 2) Push the button of "simulation-analyze trajectory" and acquire the trajectory of K^+ inside *SF*. K^+s are observed to be trans-located among the steady-states along the central axis of *SF*. 3) According to the regulation of *coulomb* repulsion and the rule of lowest free energy, continuous configurations of K^+s are combined so that

sub-conformations are deduced and clustered corresponding to varying nD_{PTTBCO}.

Abbreviation: *K*$^{+}$:potassium ion; *SF*: selectivity filter; *Slo1*:large conductance Ca^{2+}-activated potassium; *acSlo1*: *Slo1*from *Aplysia californica*;*hSlo1*: *Slo1* from human; *PTT*: potassium transportation track; *PTTBC* and $BC_{residual}$: backbone carbonyl of *PTT*, including BC_{Thr}, BC_{Val}, BC_{Gly_1}, BC_{Phe} and BC_{Gly_2}; *PTTBCO* and $BCO_{residual}$: oxygen atom of *PTTBC* including BCO_{Thr}, BCO_{Val}, BCO_{Gly_1}, BCO_{Phe} and BCO_{Gly_2}; *PR*: polarity residuals; *nPR*: non-polarity residual; $L_{Thr.OH}$, L_{Thr}, L_{Val}, L_{Gly_1}, L_{Phe}, L_{Gly_2}: six layer along central axis of *SF* from intercellular to extracellular; D_{layer}: distance of each pair of layers; D_{PTTBCO}: distance of neighbor *PTTBCOs* in a *PTT*; nD_{PTTBCO}: border length of the quadrangle which is comprised with cross-links of neighbor *PTTBCOs* in each layer; dD_{PTTBCO}: distance of two *PTTBCOs* located at diagonal *PTTs*; $ZL_{BCO_{Val}-BCO_{Gly_1}}$: a zigzag line of BCO_{Thr} and BCO_{Val} and BCO_{Gly_1}; $ZL_{BCO_{Phe}-BCO_{Gly1}}$: a zigzag line of BCO_{Gly_1} and BCO_{Phe} and BCO_{Gly_2}; C_{Thr}, C_{Val}, C_{Gly_1}, C_{Phe}, C_{Gly_2}: circle-cross-links in each layer; S_{Thr}, S_{Val}, S_{Gly_1}, S_{Phe}: 4 *stable-state-sites* which are located along center axis of *SF*, corresponding to four layer of L_{Thr}, L_{Val}, L_{Gly_1} and L_{Phe}; $S_{Thr.OH-Thr}$, $S_{Thr-Val}$, $S_{Val-\mathrm{Gly}_1}$, S_{Gly_1-Phe}, $S_{Phe-Gly_2}$: 5

meta-stable-state-sites which are located along the center axis of *SF*; *DIEP*: Delocalization ion electron pair; *ESR*: electron spin resonance; *2D IR*: two-dimensional infrared spectroscopy; *MD*: molecular dynamics.

Acknowledgment: This work was supported by National Science Foundation of China (No. 31771191, 31571032 and 81603410). The authors thank Dr. Zhirui LIU, Dr. Jie TAO, Dr. Bing WU and Dr. You ZHOU for their advices on this work. Theoretical deduction of the K^+ moving through *SF* was calculated by Miss Ziyu Guo.

Competing financial interests

The authors declare no competing financial interests.

Supplementary Information: 1) The homologous similarity alignment for the full-length *hSlo1* and *acSlo1* channels. 2) *PTTBCO* polarization and electro-negativity ($\delta\chi$). 3) Theoretical deduction of the K^+ moving through *SF*.

Author Contributions

JK GUO designed and performed the experiments and wrote the manuscript; ZY TAN contributed to the manuscript; YH JI proposed the idea and contributed to the manuscript. All authors discussed about the experiments.

Reference

[1] B. Hille, Potassium channels in myelinated nerve. Selective permeability to small cations. J. Gen. Physiol. 1973, 61, 669 – 686.

[2] C. M. Armstrong, Interaction of tetraethylammonium ion derivatives with the potassium channels of giant axons. J. Gen. Physiol. 1971, 58, 413 – 437.

[3] Heginbotham, L., Lu, Z., Abramson, T. and MacKinnon, R. Mutations in the K^+ Channel Signature Sequence (1994) Biophys. J. 66, 1061-1067.

[4] Zhe Lu and Roderick Mackinnon: A Conductance Maximum Observed in an Inward-Rectifier Potassium Channel. J. GEN. Physiol. Volume 104 September 1994, 477-486.

[5] R. MacKinnon, Pore loops: an emerging theme in ion channel structure. Neuron 1995, 14, 889 – 892

[6] R. MacKinnon, Determination of the subunit stoichiometry of a voltage activated potassium channel. Nature 1991, 350, 232 – 235.

[7] Y. Zhou, J. H. Morais-Cabral, A. Kaufman, R. MacKinnon, Chemistry of ion coordination and hydration revealed by a K^+ channel–Fab complex at 2.0 _ resolution. Nature 2001, 414, 43 – 48.

[8] Y. Zhou, R. MacKinnon, The occupancy of ions in the K^+ selectivity filter: Charge balance and coupling of ion binding to a protein conformational change underlie high conduction rates. J. Mol. Biol. 2003, 333, 965 – 975.

[9] D. A. Doyle, J. H. Morais Cabral, R. A. Pfuetzner, A. Kuo, J. M. Gulbis, S. L. Cohen, B. T. Chait, R. MacKinnon, The structure of the potassium channel: molecular basis of K^+ conduction and selectivity. Science 1998, 280, 69 – 77.

[10] J. H. Morais-Cabral, Y. Zhou, R. MacKinnon, Energetic optimization of ion conduction rate by the K^+ selectivity filter. Nature 2001, 414, 37 – 42.

[11] Dassault systèmes BIOVIA， Discovery Studio Modeling Environment, Release 2017, San Diego, Dassault systèmes 2016.

[12] Xiao Tao, Richard K. Hite, and Roderick MacKinnon: Cryo-EM structure of the open high conductance Ca^{2+}-activated K^+ channel. Nature. 2017 January 05; 541(7635): 46–51.

[13] Alcayaga C, Cecchi X, Alvarez O, Latorre R. Streaming potential measurements in Ca^{2+}-activated K^+ channels from skeletal and smooth muscle. Coupling of ion and water fluxes. Biophys J. 1989 Feb; 55(2): 367-71.

[14] Yifrach O, MacKinnon R.: Energetic of pore opening in a voltage-gated K^+ channel. Cell. 2002 Oct 18; 111(2):231-9.

[15] George Eisenman, Ramon Latorre, Christopher Miller: Multi-ion conduction and selectivity in the high-conductance Ca^{2+}-activated K^+ channel from skeletal muscle. Biophys. J., Volume 50 December 1986 1025-1034.

[16] Huong T. Kratochvil, Joshua K. Carr, Kimberly Matulef and etc. Instantaneous ion configurations in the K^+ ion channel selectivity filter revealed by *2D IR* spectroscopy. Science. 2016 September 02; 353(6303): 1040–1044.

[17] Zhou M, MacKinnon R. A mutant KcsA K^+ channel with altered conduction properties and selectivity filter ion distribution. J Mol Biol. 2004 May 7; 338(4): 839-46.

[18] Nernst, W. Zur Kinetik der in L.sung befindlichen K.rper. *Z. Phys. Chem. 2*:613–637. 1888. http://dx.doi.org/10.1515/zpch-1888-0174.

[19] Planck, M. Ueber die Erregung von Elektricit. t und W.rme in Elektrolyten. *Ann.Phys.2*75:161–186.1890.http://dx.doi.org/10.1002/and p .18902750202.

[20] Hodgkin A.L., and A.F. Huxley. A quantitative description of membrane current and its application to conduction and excitation in muscle. *J. Physiol.* 117:500–544. 1952.

[21] Hodgkin, A.L., KATZ B. The effect of sodium ions on the electrical activity of giant axon of the squid. J Physiol. 1949 Mar 1; 108(1):37-77.

TOC graph:

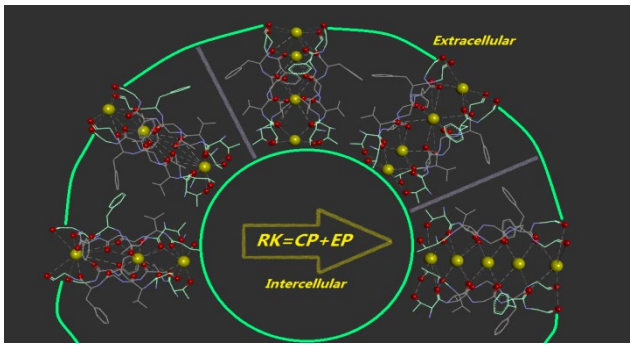

Three patterns of K^+ passing through the membrane channel were found under diffusion force of ion concentration and electric potential on cellular membrane. To accommodate increasing energy levels, 4-fold symmetric subunits of the channel can only move at one direction that is perpendicular to the centre axis, and tolerate more K^+.